Akaganeite polymer nanocomposites

A. Millan [a,*], A. Urtizberea [a], E. Natividad [a], F. Luis [a], N.J.O. Silva [a], F. Palacio [a], I. Mayoral [a], M.L. Ruiz-González [b], J.M. González-Calbet [b], P. Lecante [c], V. Serin [c]

[a] *Instituto de Ciencia de Materiales de Aragón, CSIC-Universidad de Zaragoza, Facultad de Ciencias, Pza. San Francisco s/n, 50009 Zaragoza, Spain*
[b] *Dpto. Química Inorgánica, Universidad Complutense de Madrid, 28040 Madrid, Spain*
[c] *CEMES-CNRS, 29 rue Jeanne Marvig, F-31055 Toulouse Cédex, France*
E-mail address: amillan@unizar.es (A. Millan).

Abstract

An "in situ" method for the production of akaganeite polymer nanocomposites is described. A controlled precipitation is achieved by using a polymer matrix, polyvinylpyridine, containing *N*-base functional groups that form coordination bonds with iron ions. The resulting materials have permitted the obser- vation of two sources of magnetic moment in akaganeite nanoparticles: (1) finite size effects with a characteristic blocking temperature below 2 K; and (2) a deficient Cl^- occupancy, with a characteristic blocking temperature around 18 K. Moreover, the nanocomposites can be dissolved in slightly acidic media to obtain stable aqueous nanoparticle dispersions that could be useful in biomedical applications

1. Introduction

In their several crystalline forms, iron oxides are valuable materials for a variety of applications [1]. In particular, akaganeite (β-FeOOH) is present in pharmaceutical formulations for the treatment of anaemia [2]. It is also used in environmental applications [3,4] and catalysis [5], thanks to its capacity for ion and vapour adsorption. Though not frequently, akaganeite is found in soils [6,7], and possibly in other planets [8]. Moreover, akaganeite is used as a precursor in the production of other iron oxide phases such as hematite [9], goethite [10], and magnetite [11], in order to obtain particle morphologies that are unusual in these iron oxide phases. In this way, akaganeite is indirectly useful in industrial and biomedical applications associated to other iron oxide phases. Besides industrial applications, akaganeite is also interesting in basic science, mainly in geology, corrosion, colloids and magnetism. For instance, an open issue in magnetism is the variation of magnetic properties of bulk materials when their size is reduced to the nanometer range. This phenomenon has been extensively studied in ferromagnetic materials but rarely in antiferromagnetic ones. As a characteristic antiferromagnet, akaganeite can be a suitable model material in these studies. For this purpose, nanocomposites would be the ideal samples, since particles should be isolated in order to distinguish between intrinsic particle properties and collective effects.

Akaganeite has a monoclinic crystal structure [12,13] formed by square channels of double octahedra chains that are held by interstitial Cl^- ions. The content of Cl^- ions in these channels varies with the preparation method [1,14–20], it can be exchanged with other ions [14–18], and it can be washed out with water [18–20]. The mobility of Cl^- ions along the square channels and the capacity for ion adsorption make akaganeite specially suitable for catalysis and ion exchange applications [15,18,21]. When the Cl^- content decreases below a threshold the structure transforms into goethite [1,16,21,22].

Akaganeite is usually prepared by the hydrolysis of $FeCl_3$ aqueous solutions at moderate temperatures. The pH must be slightly acidic ($pH < 5$) to avoid the formation of more stable phases, such as hematite and goethite [23]. Akaganeite has also been obtained by hydrothermal synthesis [24], and by the addition of NaOH to $FeCl_2$ solutions [22]. For all these methods, particles are usually rod-like single crystals with a length of several tenths of micron [25] that, concerning magnetic properties, can be considered as bulky particles. Some additives and organic solvents [26–30] may induce the formation of akaganeite at a high pH. In these conditions, the particle size is reduced to a few nanometers, and aggregation is promoted.

A convenient method to control aggregation and particle size would be to prepare akaganeite particles in a template, such as a polymer. However, there are few examples of akaganeite polymer nanocomposites in the literature. Dextran and other polysaccharides have often been used, mainly because they are an adequate embodiment for biomedical applications, such as anaemia therapy [29,31–34]. Other matrixes used for akaganeite nanocomposites are assemblies of polyions [35], and nanoporous alumina [36].

This report focuses on the preparation of akaganeite–polymer nanocomposites that can be used in studies of the magnetic properties of antiferromagnetic nanoparticles as well as in biomedical and industrial applications. Among the numerous routes to prepare magnetic polymer nanocomposites [37], in situ precipitation has been our choice, since it yields homogeneous materials and profits from the moulding effect of the polymer. In this route, the matrix is mixed with a molecular metal precursor and the particles are grown inside the precursor-polymer compound by the addition of a precipitating agent [38]. The polymer used here is poly(4-vinylpyridine) (PVP), that has nitrogen base groups that form coordination bonds with iron ions. In this way, the hydrolysis reaction is carried out in a controlled manner. This method has recently been employed for the production of maghemite nanocomposites with success [39]. In that case, the precipitating agent was sodium hydroxide, and the precursor salt was iron bromide. In the present case, the precipitating agent is the same, while the precursor is iron chloride. The nanocomposites can be readily dissolved in slightly acidic media to obtain aqueous nanoparticle dispersions. The obtained nanocomposites have been employed in detailed magnetic studies that will be described in a future paper. Nevertheless, beyond the report of the nano- composites synthesis, some novel features about akaganeite magnetic behaviour concerning the influence of Cl^- ions are advanced in this report.

2. Experiments

Inorganic reagents and PVP polymer (60000 D) were purchased from Aldrich.

Gels of iron–PVP coordination compounds were prepared by dissolving 0.2 g of PVP in 4 mL of water/acetone (1:1); mixing this solution with 2 mL of 1 M $FeCl_3$\$$6H_2O$ solution in the same solvent; and drying first in air and then in an oven at 60 C for 2 h.

Akaganeite nanocomposites were prepared by immersing the iron–PVP coordination compound in a volume of 1 M NaOH solution for a Fe/OH ratio of 1:3; washing with water; and drying at room temperature, and then in an oven at 150 C. Two nanocomposite samples were prepared by the procedure described in the experimental section with a [Fe]/[pyridine] ratio = 1.05. The first sample, NC_{wash}, was extensively washed with water after the treatment with NaOH, whereas the second sample, NC_{Cl}, was just slightly washed. Bulk akaganeite powders were prepared by aging a 1 M $FeCl_2$ solution during one month in an oven at 70ºC.

Iron content in the samples was determined in a Perkin–Elmer Plasma 40. X-ray powder diffraction (XRD) was performed in a Rigaku D-max B diffractometer. Fourier Transform Infrared (FTIR) spectra were taken on KBr pellets using a Perkin Elmer Spectrum One instrument.

Transmission electron microscopy (TEM) was performed with a Jeol-2000 FXII microscope, with point-to-point and line-to-line resolutions of 2.8 Å and 1.4 Å, respectively. Samples for TEM observations were prepared in two different ways: (1) grounding the nanocomposites in acetone and evaporating drops of the suspension on carbon-coated copper grids; and (2) embedding the grounded composite in an epoxy resin and cutting ultrathin slices by ultramicrotomy. Both low and high-magnification images were recorded, the latter revealing details of the crystallite structure. Nanocomposite samples for small-angle X-ray scattering (SAXS) measurements were prepared by grounding the as prepared films in a mortar and then pressing the grains into pellets having an approximate thickness of 0.2 mm. SAXS experiments were carried out at the beam line ID01 of the European Synchrotron Radiation Facility (ESRF). Magnetic characterization including ac suscepti bility and magnetization versus field measurements were per formed in a SQUID MPMS magnetometer from Quantum Design.

3. Results and discussion

3.1. XRD and FTIR characterization

Fig. 1 shows XRD patterns from NC_{wash} and NC_{Cl} composite samples, PVP polymer, and precipitated akaganeite powders. The nanocomposite XRD patterns show a very broad peak around 20º , which is also observed in the polymer pattern, and some narrower peaks, which are in turn present in akaganeite powder pattern, at angles corresponding to those of akaganeite crystal structure. The differences in relative peak intensities between powders and nanocomposites patterns and the reference pattern are probably due to particle shape effects. The pattern of sample NC_{Cl} shows additional sharp peaks that correspond to NaCl crystal structure revealing that the washing was insufficient to eliminate this salt from the nanocomposite. An analysis by atomic absorption yielded 22 wt% of Fe and 4 wt% of Na in this sample.

Fig. 2 shows FTIR spectra of pure akaganeite powders, PVP and nanocomposite samples. The spectrum of akaganeite powders shows broad bands at 1623 cm^{-1}, 850 cm^{-1}, 683 cm^{-1}, and 411 cm^{-1}, and shoulders at 630 cm^{-1} and 473 cm^{-1}, which are close to wave number values reported for this compound [20–40]. The band at 1623 cm^{-1} can be assigned to bending vibrations of structural water bound to different sites [41,42]. The band at 850 cm^{-1} and shoulder at 630 cm^{-1} correspond to H–O–Cl libration modes (850 + 826 cm^{-1}, 642 cm^{-1} in Refs. [20,43]). The shoulder at 473 cm^{-1} and the strong band at 411 cm^{-1} can be related to Fe–O translational modes (479, 424 cm^{-1} in Ref. [43]), or to Fe–O–Fe symmetric stretching vibrations [42,44]. The band at 683 cm^{-1}, often assigned to OH libration modes, has recently been considered as an artefact [44]. Actually, there is some disparity between reported values for akaganeite IR bands that can be due to different Cl^- content in the samples [20]. For instance, Ref. [28] reports

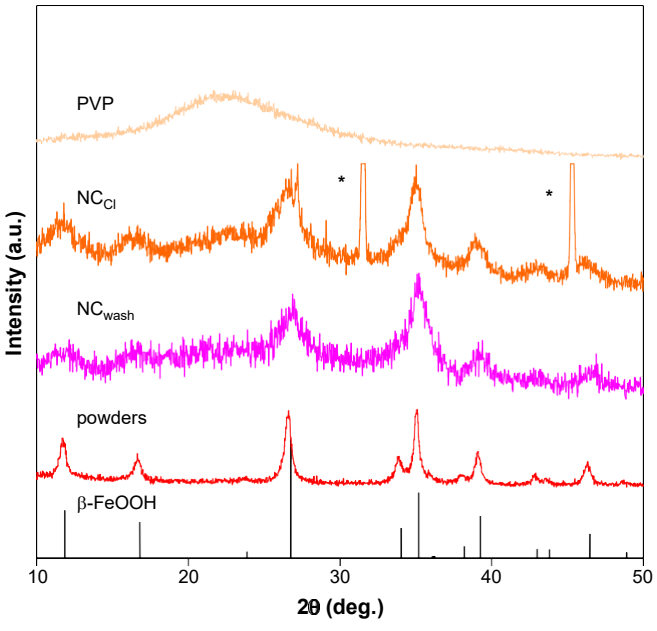

Fig. 1. XRD patterns of akaganeite database reference (β-FeOOH), akaganeite nanoparticle powders from spontaneous precipitation, nanocomposite samples NC_{wash} and NC_{Cl}, and PVP polymer. Peaks marked with (*) correspond to NaCl crystal structure.

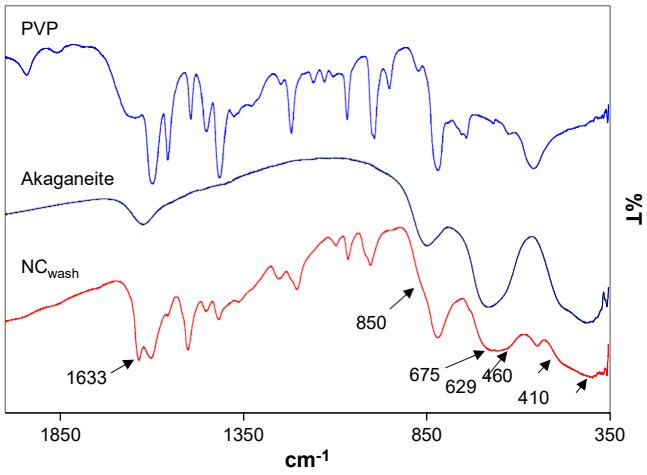

Fig. 2. FTIR spectra of nanocomposite sample NC_{wash}, akaganeite nanoparticle powders from spontaneous precipitation and PVP polymer.

bands at 850+ 820 cm^{-1}, 650 cm^{-1}, 487 cm^{-1} and 420 cm^{-1}, whereas Ref. [27] finds bands at 848 cm^{-1}, 633 cm^{-1} and 404 cm^{-1}. The spectrum of the nanocomposite sample can be interpreted as sum of polymer and powder spectra. Characteristic bands of akaganeite powders are clearly distinguishable, as indicated in Fig.2. No bands are observed from any other iron oxide phase apart from akaganeite.

3.2. TEM observations

Fig. 3 shows a TEM image of akaganeite nanocomposite sample NC_{wash} after grinding in a mortar. The particle density is very high, and therefore particle shape is only distinguished on the grain edges. The image shows rod-like particles with average length and thickness 24±5 nm (mean SD) and 5±1 nm, respectively.

These dimensions are smaller than those found in akaganeite powders from slow hydrolysis of iron(III) chloride solutions, whose typical dimensions are between 0.2 and 0.5 mm in length and 0.02–0.1 in width [1]. Fig. 4 shows a TEM image of a grinded sample NC_{Cl}. The particles are also rod-like with average length and width 18 6 and 5 1 nm, respectively. The Cl/Fe atomic ratios in NC_{wash} and NC_{Cl} samples estimated by energy dispersive spectrometry (EDS) were 0.3 and 0.8, respectively, indicating that washing effectively removed Cl^- ions from the akaganeite nanoparticles.

High-magnification images enabled us to measure the interplanar atomic distances of nanoparticles with different orienta tions. One of these images is shown in Fig. 5. Lattice plane distances of 1.87, 2.03 and 2.62/2.66 Å were measured, corresponding to (4 4 0), (1 5 0) and (4 0 0) planes of akaganeite crystal structure [13]. Analysis of different nanoparticle images yields other distances, such as 2.35/2.36, 2.79/2.80 and 3.02/3.03 Å that can be assigned to (2 4 0), (1 1 1) and (0 0 1) planes.

In order to determine the disposition of the particles within the matrix, ultrathin slices of sample NC_{Cl} were observed by TEM as shown in Fig. 6. It is observed that, at short length scales, the particles are arranged parallel, forming sheets.

3.3. SAXS analysis

The nanostructure of composite samples was examined by SAXS following a procedure similar to that previously applied to maghemite/PVP nanocomposites [45]. Fig. 7 shows SAXS plots of pellets of powdered polymer and composite samples double-logarithmic scale. The polymer curve shows a region of constant intensity at higher q values, implying that the structure is homogeneous in the corresponding length scale. At lower q values, the scattered intensity follows a region of linear increase with a slope of 3.3. This power-law behaviour is not far from the typical scattering behaviour of smooth surfaces (n= 4), usually referred as Porod

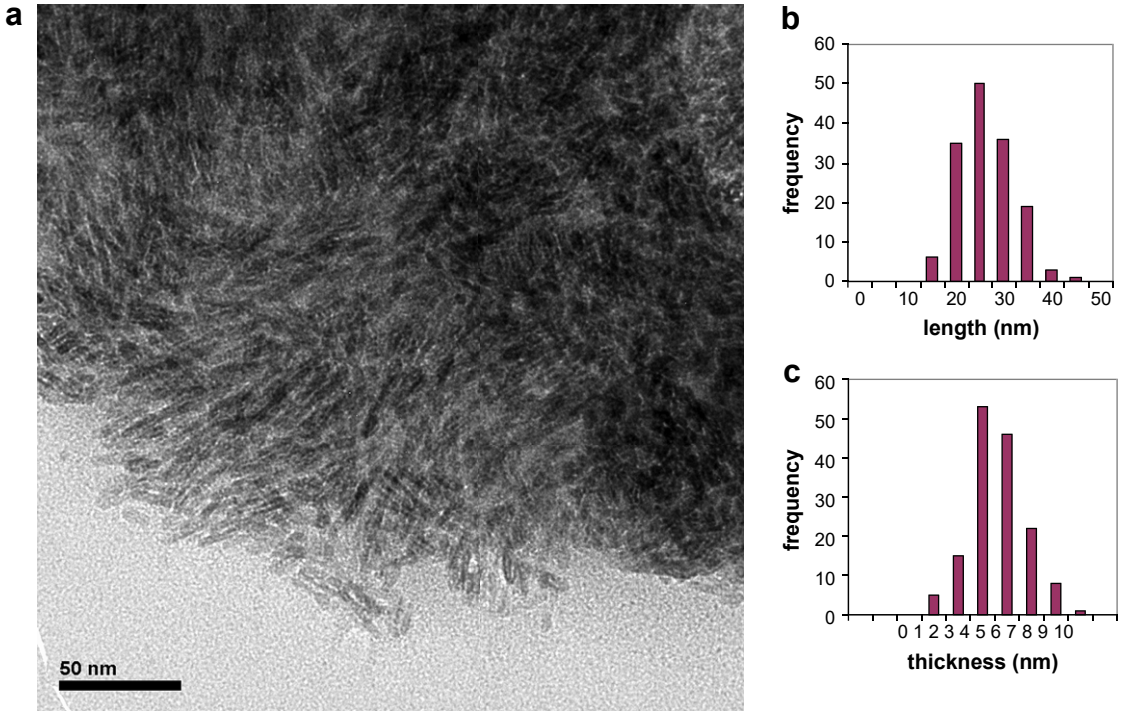

Fig. 3. TEM image of grinded akaganeite/PVP nanocomposite sample NC_{wash} (a), and histograms of particle length (b) and width (c).

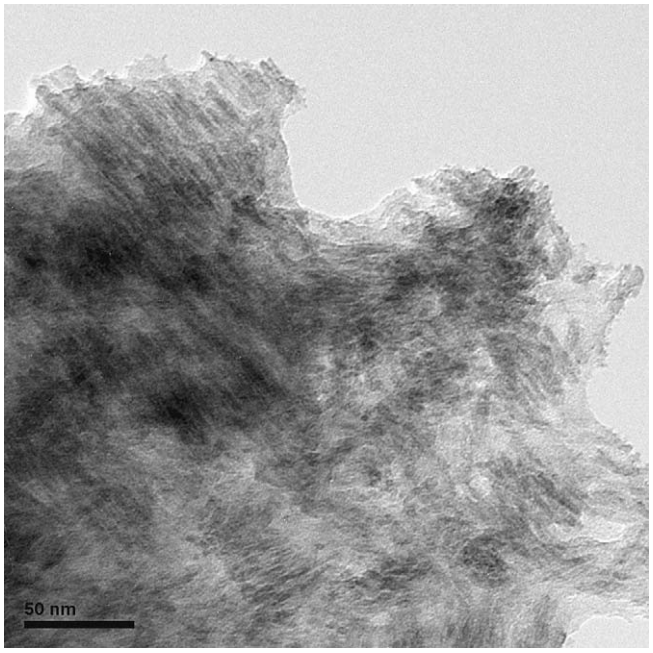

Fig. 4. TEM image of grinded akaganeite/PVP nanocomposite sample NC_{Cl}.

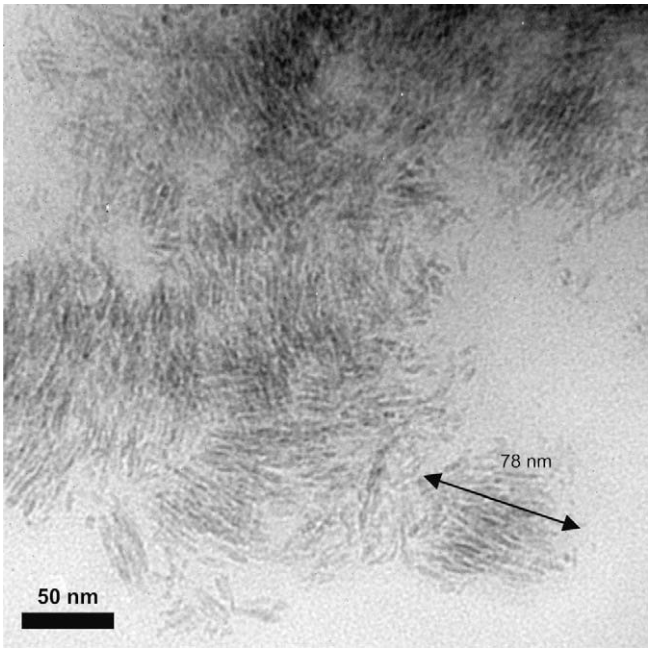

Fig. 6. TEM image of an ultrathin slice of akaganeite/PVP nanocomposite sample NC_{Cl}.

regime [46], and can be assigned to surface scattering from folded polymer chains [45]. The SAXS curves of the two nanocomposite samples are very similar to each other, consisting of a region of steep linear increase at higher q values followed by another region of linear increase with a lower slope. As in previous SAXS analysis [45], it can be considered that the observed intensity is the sum of polymer and particle contributions. Fig. 7b represents the scattering intensity after subtracting the contribution of the polymer for sample NC_{Cl}. The plot shows a central region of linear increase with a slope n = 2.0, which is usually associated to tabular objects, and not a slope n = 1, expected for rod-like particles. At the same time, the cross-over points at the beginning and end of central linear region corresponds to characteristic distances of the tabular objects of 6 and 73 nm. These tabular objects could correspond to the planar arrays of acicular particles, observed in TEM images. In fact, the first distance is close to the average particle thickness determined by TEM and consequently to the height of tabular objects, while the ending distance is clearly higher than particle length but it is comparable to the width of these objects (Fig. 6).

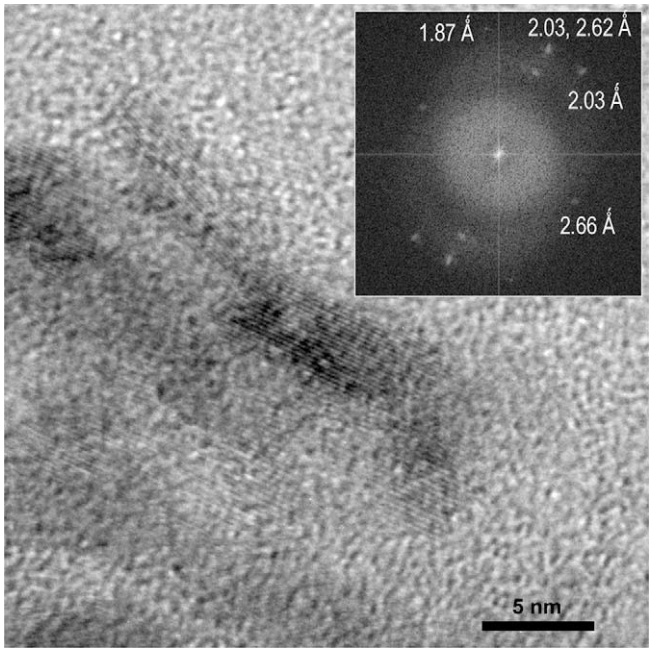

Fig. 5. HRTEM image of a bunch of nearly parallel needle particles showing the same direction of elongation. In the inset, electron diffraction pattern of the area.

3.4. Mechanisms of particle formation

The hydrolysis of iron ions may lead to a variety of crystalline phases depending on the precipitation conditions and the precursor iron salt, by a process that involves several intermediate iron species. Concerning the akaganeite phase, it is formed in iron aqueous solutions only under the following conditions: in the presence of chloride ions, slightly acidic solutions, and moderate temperatures. Nucleation and growth proceed by two different hydrolysis reactions, namely olation and oxolation. The process has been explained by Bottero et al. [47] and it can be summarized as follows: (1) formation of iron dimers and trimers (2) condensation into Fe24 polycations (with the same local structure as akaganeite), (3) arrangement of Fe24 clusters into linear chains, (4) chain ramification, (5) precipitation of hydrated low density amorphous particles, (6) condensation into crystalline particles. Obviously, it is difficult to control this process, although it is known that it is drastically affected by the presence of iron ligands, such as PO_4^{3-} [48]. The strategy proposed here to control akaganeite precipitation is to perform the process in a restrictive environment.

There are three factors that may contribute to growth restriction in iron–PVP system: (1) the growth medium is a solid matrix and therefore ion diffusion is slowed down with respect to liquid media, (2) the matrix contains pyridine groups that interact with iron growing units and with the particle surface by means of N–Fe coordination bonds, and (3) the pyridine groups are protonized before the onset of precipitation, becoming hydrophobic. This third factor can be determinant on particle growth process. As it is explained in our previous report [39], the initially homogeneous

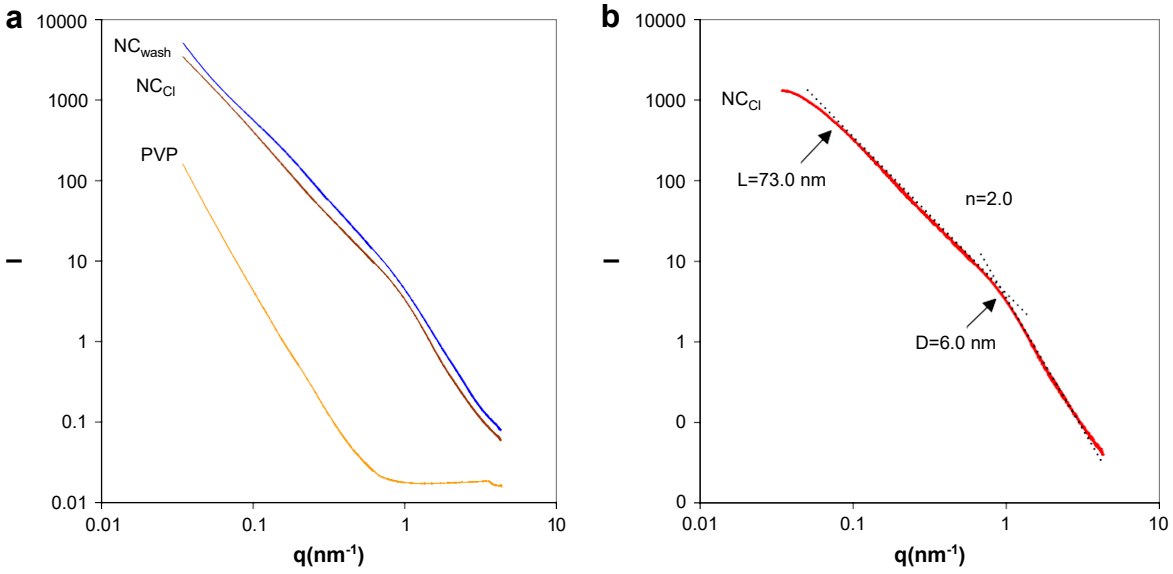

Fig. 7. a) SAXS log plots of pellet samples of poly(4-vinylpyridine) polymer (PVP) and akaganeite/PVP nanocomposite samples NC_{wash} and NC_{Cl}; (b) SAXS curve of NC_{Cl} sample after subtracting the polymer scattering.

iron–polymer gel collapses when the pyridine groups become hydrophobic. The new microstructure would be no longer uniform in the nanometer scale, but most probably it would be partitioned into hydrophilic and hydrophobic regions encapsulating the iron ions. Thus, the subsequent growth process will be restricted by the amount of iron ions contained in each hydrophilic region. This mechanism explains the small particle size and the absence of aggregates. Besides, it will help to reduce the particle size dispersion.

3.5. Magnetic properties

Fig. 8 shows the variation of magnetization with the applied field, H, for NC_{wash} and NC_{Cl} samples. Curves from both samples show the presence of a contribution saturating at relatively low magnetic fields plus another contribution that increases approximately linearly with H. The former contribution is larger for NC_{wash} sample than NC_{Cl}. In fact, at high fields ($H > 30\,000$ Oe) NC_{Cl} curve is almost linear as expected for a perfect antiferromagnet, whereas NC_{wash} still shows a slight curvature, indicating the pres- ence of a small magnetic moment in the particles.

Fig. 9 shows plots of in-phase, χ', and out-of-phase, χ'', ac susceptibility components, respectively, for composite and powder samples. χ'' is zero over the whole temperature range for the powder. Consequently, there is not a relaxation phenomenon associated to bulk antiferromagnetic akaganeite that might become noticeable within the measuring temperature range. Sample NC_{Cl} shows a similar behaviour down to 20 K. However, below 20 K and for decreasing temperatures, χ' increases steeply, χ'' increases constantly from zero, and both of them depend on frequency. This suggests the appearance of a slow magnetic relaxation phenom- enon due to finite size effects. In a first instance, this phenomenon could be associated with a small magnetic moment arising from uncompensated surface spins. Sample NC_{wash} shows a more complex behaviour. χ' and χ'' show a peak around 20 K, and they become frequency dependent at 70 K already. Moreover, equilibrium magnetic susceptibility of NC_{wash} is clearly larger than equilibrium susceptibility of NC_{Cl} (per unit of FeOOH mass). Thus, the former sample has an additional source of uncompensated magnetic moment with respect to the latter one, which is in agreement with magnetization results. The additional contribution to χ' apparently vanishes below 5 K. Indeed, below 5 K, χ' and χ'' data are fairly coincident in both samples. This suggests that the additional moment in NC_{wash} blocks at a higher blocking temperature, T_b. Therefore, it is associated with a slower relaxation process or with a higher magnetic anisotropy. Notice that, according to EM and SAXS measurements, particle sizes are similar, and therefore this additional moment and longer relaxation is not likely associated with differences in particle sizes between the two composites. In order to confirm this point, TEM observations and magnetic measurements in both samples were repeated with identical results. Therefore, the structural feature determining the differences in magnetic behaviour between the samples must arise from the washing process.

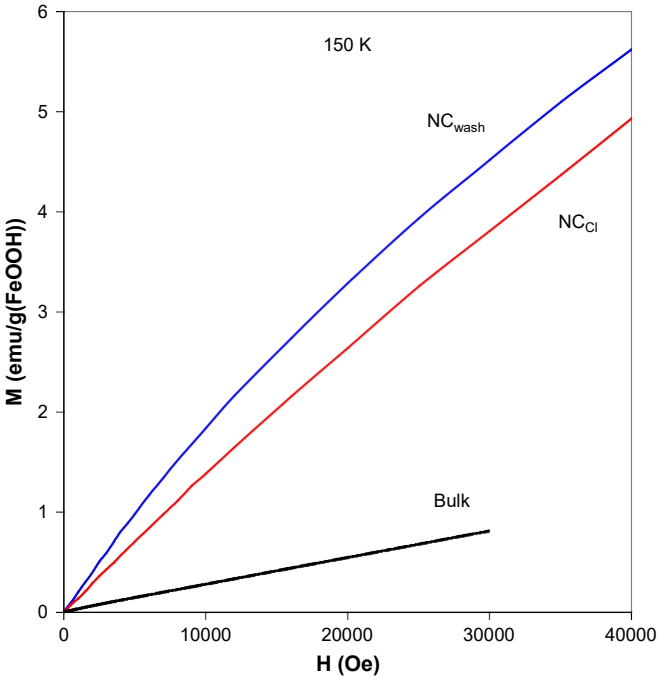

Fig. 8. Field dependence of the magnetization of akaganeite bulk and akaganeite nanocomposite samples NC_{wash} and NC_{Cl} at 150 K.

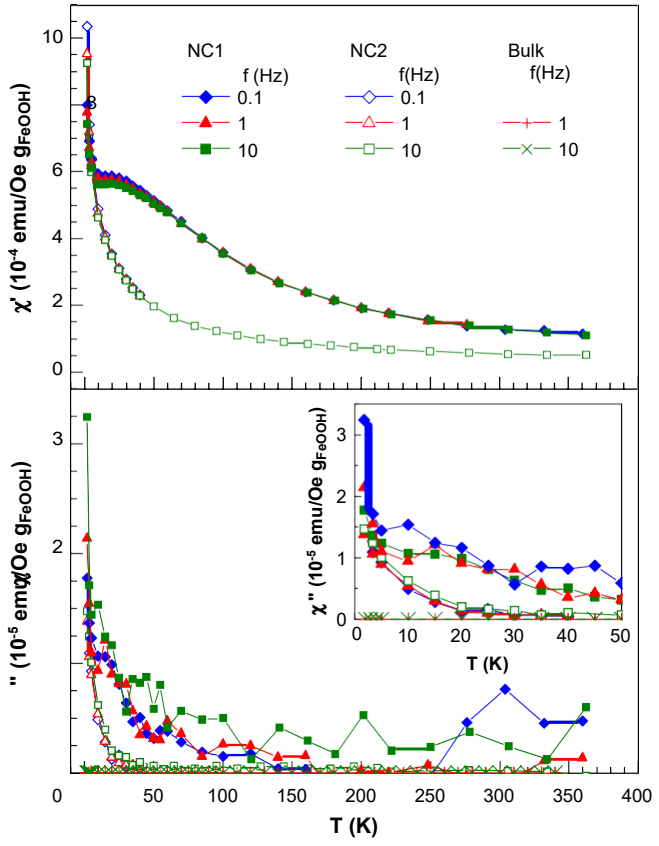

Fig. 9. Temperature dependence of in-phase (χ'), and out-of-phase (χ'') ac magnetic susceptibility of akaganeite powders (bulk), and nanocomposite samples NC_{wash} and NC_{Cl}.

It has been pointed out in the intro- duction section that washing with pure water or with solutions containing small anions can produce a release of Cl^- ions from akaganeite crystal structure. It has been estimated that most of exchange sites are tunnel sites and only a 13% are surface sites [18,21]. Thus, it is reasonable to assume that the content of inter- stitial Cl^- ions in NC_{wash} sample will be decreased in comparison with that of NC_{Cl} sample. An incomplete filling of Cl^- sites may alter the perfect compensation of antiferromagnetic sublattices, and consequently it may lead to the appearance of an associated magnetic moment. In other words, Cl^- ions play a role in magnetic exchange interactions and a perfect sublattice alignment is only achieved when the crystal lattice is saturated with Cl^- ions. The effect of Cl^- deficiency on the magnetic properties of akaganeite has been outlined before [49] in relation to a decrease of Néel temperature, T_N. However, other authors attribute this decrease to an increment of the water content [50].

Reports on ac measurements of akaganeite nanoparticles describe susceptibilities χ' and χ'' that increase with the tempera- ture find a maximum around 10 K (T_b = 8 K, 11 K) and decrease again [34]. The measured samples were commercial iron dextran preparations containing particles with an approximate size of 20x4 nm. Studies based on ZFC-FC dc susceptibility measure- ments, yielded T_b = 18 K for spherical particles [22], and T_b = 15 K for two different rod-like particle samples with sizes 120x 25 nm and 200x50 nm respectively [36], and they also showed a constant decrease of susceptibility at temperatures below T_b. Muon spin relaxation experiments (measuring time, $\tau_m = 10^{-8}$ s) yielded a blocking temperature of 10 K on akaganeite nanoparticles with an average size of 6 nm [52]. By contrast, much higher T_b values (150–290 K in [40] and 65–215 K in [41]) have been derived in Mössbauer measurements from doublet-to-sextet conversions.

However, these conversions have also been interpreted as an order–disorder magnetic transition (T_N) [51], in agreement with our own measurements that indicate Néel temperatures in the range between 220 K and 250 K [to be published]. Thus, studies of relaxation phenomena in akaganeite nanoparticles with a size of the same order of those studied here yield T_b values in the range 8–18 K that are usually related to small magnetic moments originated from uncompensated spin lattices on particle surface [53].

However, we have observed that nanoparticle samples that have not been thoroughly washed after synthesis, ensuring a full Cl^- site occupation, show relaxation effects with an associated T_b well below these values (<2 K). On the other hand, samples undergoing a more extensive washing that may cause a structural Cl^- deficiency, at least in a part of the particle population, show an associated blocking temperature in the range of those previously reported. Since it is expected that samples used in most of previous studies were commercial and probably deeply washed with water during their preparation, the observed blocking may actually arise from a defective occupation of Cl^- crystal sites, as in our case. As a consequence, moments arising from uncompensated surface spins would have a lower blocking temperature and thus an anisotropy lower than that derived.

4. Conclusions

A method is proposed for the preparation of akaganeite nano-composites based on the use of polymers with *N*-base functional groups that form coordination bonds with transition metal ions. Akaganeite nanocomposites are prepared by the addition of a base to a uniform iron/polymer gel obtained by evaporation of iron chloride polymer solutions. The resulting nanocomposites contain rod-like nanoparticles grouped in parallel planar arrays that can be dispersed in slightly acidic media. Magnetic measurements show a small magnetic moment in akaganeite nanoparticles due to size effects that is not totally blocked at temperatures above 2 K. An additional contribution to magnetic moment appears after washing the samples that could arise from a deficient Cl^- sites occupancy. Thus, our preparation method provides access to samples with intermediate content in Cl^- which enables us to ascertain the different origins of magnetic moment in nanosized akaganeite.

Acknowledgments

Financial support was provided by research grant MAT2007-61621 from the Spanish CICYT Project Consolider-Ingenio in Molecular Nanoscience CSD2007-00010 from the Spanish Ministry of Education, and by the Communauté de Travail des Piréné es. This work was carried out in the frame of the EC NoE 'MAGMANET'.

References

[1] Cornell RM, Schwertmann U. The iron oxides. Weinheim: VCH Publishers; 1997.
[2] Coe EM, Bowen LH, Speer JA, Wang Z, Sayers DE, Bereman RD. J Inorg Biochem 1995;58:269.
[3] Cadena F, Johnson MD. US Patent 2004262225; 2004.
[4] Clarke NS, Hall PG. Langmuir 1991;7:672.
[5] Yuan ZY, Ren TZ, Su BL. Catal Today 2004;93–95:743.
[6] Holm NG, Dowler MJ, Wadstein T, Arrhenius G. Geochim Cosmochim Acta 1983;47:1465.
[7] Keller P. Neues Jahrb Miner Abh 1970;113:29.
[8] (a) Morris RV, Golden DC, Bell JF, Shelfer TD, Scheinost AC, Hinman NW, et al. J Geophys Res Planets 2000;105:1757;
(b) Buchwald VF, Clarke Jr RS. Am Mineral 1989;74:656–67.

[9] Goñi-Elizalde S, Garcia-Clavel ME, Tejedor-Tejedor MI. React Solids 1987;3:139.
[10] Cornell RM, Giovanoli R. Clay Clay Miner 1990;38:469.
[11] Blesa MA, Mijalchik M, Villegas M, Rigotti G. React Solids 1986;2:85.
[12] Stahl K, Nielsen K, Jiang J, Lebech B, Hanson JC, Norby P, et al. Corros Sci 2003;45:2563.
[13] (a) Weiser HB, Milligan WO. J Am Chem Soc 1935;57:238;
(b) Post JE, Buchwald VF. Am Mineral 1991;76:272;
(c) Post JE, Heany J, von Dreele RB, Hanson JC. Am Mineral 2003;88:782.
[14] Chambaere DG, Grave ED. Phys Status Solidi A 1984;83:93.
[15] Streat M, Hellgardt K, Newton NLR. Process Safe Environ Prot 2008;86:1.
[16] Ellis J, Giovanoli, Stumm W. Chimia 1976;30:194.
[17] Weiser HB, Milligan WO. J Phys Chem 1935:3925.
[18] Cai J, Liu J, Gao Z, Navrotsky A, Suib SL. Chem Mater 2001;13:4595.
[19] Mackay AL. Mineral Magn 1960;32:545.
[20] Deliyanni EA, Bakoyannakis DN, Zouboutis AI, Matis KA, Nalbandian L. Microporous Mesoporous Mater 2001;42:49.
[21] Paterson R, Rahman H. J Colloid Interface Sci 1983;94:60; 1984;98:494.
[22] Refait P, Génin JMR. Corros Sci 1997;39:539.
[23] Bao H, Koch PL. Geochim Cosmochim Acta 1999;63:599;
Atkinson RJ, Posner AM, Quirk JP. Clay Clay Miner 1977;25:49.
[24] Riveros PA, Dutrizac JE. Hydrometallurgy 1997;46:85.
[25] Bailey JK, Brinker CJ, Mecartney ML. J Colloid Interface Sci 1993;157:1.
[26] Yuan ZY, Su BL. Chem Phys Lett 2003;381:710.
[27] Saric A, Nomura K, Ljubesic N, Popovic S, Music S. Mater Chem Phys B 1998;52:214.
[28] Bakoyannakis DN, Deliyanni EA, Zouboulis AI, Matis KA, Nalbandian L, Kehagias T. Microporous Mesoporous Mater 2003;59:35.
[29] Nesterova M, Moreau J, Banfield JF. Geochim Cosmochim Acta 2003;67:1177.
[30] Fan H, Song B, Yang Z, Li Q. Chem Lett 2004;33:576.
[31] Sun ZY, Huang JB. Acta Phys Chim Sin 2006;22:172.
[32] Knight B, Bowen LH, Bereman RD, Huang S, De Grave E. J Inorg Biochem 1999;73:227.
[33] Funk F, Long GJ, Hautot D, Büchi R, Christl I, Weidler PG. Hyperfine Interact 2001;136:73.
[34] Lázaro FJ, Larrea A, Abadía AR. J Magn Magn Mater 2003;257:346.
[35] Dante S, Hou ZZ, Risbud S, Stroeve P. Langmuir 1999;15:2176.
[36] Zhang LY, Xue DS, Fen J. J Magn Magn Mater 2006;305:228.
[37] Millán A, Palacio F, Snoeck E, Serin V, Lecante P. In: Mai YW, Yu ZZ, editors. Polymer nanocomposites. Cambridge: Woodhead Publishing Ltd; 2006. p. 441.
[38] (a) Castro C, Millan A, Palacio F. J Mater Chem 2000;10:1945;
(b) Ramos J, Millan A, Palacio F. Polymer 2000;41:8461;
(c) Castro C, Ramos J, Millan A, González-Calbet JM, Palacio F. Chem Mater 2000;12:3681;
(d) Millan A, Palacio F. Appl Organomet Chem 2001;15:3681.
[39] Millan A, Palacio F, Falqui A, Snoeck E, Serin V, Bhattacharjee A, et al. Acta Mater 2007;55:2201.
[40] Wolska E. Solid State Ionics 1988;28–30:1349.
[41] Murad E, Bishop JL. Am Mineral 2000;85:716.
[42] González-Calbet JM, Alario-Franco MA, Gayoso-Andrade M. J Inorg Nucl Chem 1981;43:257.
[43] Weckler B, Lutz HD. Eur J Solid State Inorg Chem 1998;35:531.
[44] Saric A, Music S, Nomura K, Popovic S. Mater Sci Eng B 1998;56:43.
[45] Millan A, Urtizberea A, Silva NJD, Boesecke P, Natividad E, Palacio F, et al. J Appl Crystallogr 2007;40:s696.
[46] Porod G. Kolloid Z 1951;124:83.
[47] Bottero JY, Manceau A, Villieras F, Tchoubars D. Langmuir 1994;10:316.
[48] Rose J, Manceau A, Bottero JY, Masion A, Garcia F. Langmuir 1996;12:6701.
[49] Barrero CA, Garcia KE, Morales AL, Kodjikian S, Greneche JM. J Phys Condens Mater 2006;18:6827.
[50] Chambaere DG, Grave ED. Phys Chem Miner 1985;12:176.
[51] Chambaere DG, Grave ED. J Magn Magn Mater 1984;42:263.
[52] van Lierop J, Ryan DH, Pumarol ME, Roseman M. J Appl Physiol 2001;89:7645.
[53] Néel L. J Phys Soc Jpn 1962;17(Suppl. B-I):676.